A Central Indian Ocean Mode and Heavy Precipitation during the Indian Summer Monsoon

LEI ZHOU

State Key Laboratory of Satellite Ocean Environment Dynamics, Second Institute of Oceanography, Hangzhou, China

RAGHU MURTUGUDDE

University of Maryland, College Park, College Park, Maryland

DAKE CHEN

State Key Laboratory of Satellite Ocean Environment Dynamics, Second Institute of Oceanography, Hangzhou, China

YOUMIN TANG

State Key Laboratory of Satellite Ocean Environment Dynamics, Second Institute of Oceanography, Hangzhou, China, and Environmental Science and Engineering, University of Northern British Columbia, Prince George, British Columbia, Canada

(Manuscript received 29 April 2016, in final form 1 December 2016)

ABSTRACT

A central Indian Ocean (CIO) mode is found to play a critical role in driving the heavy precipitation during the Indian summer monsoon (ISM). It is typically denoted with a combination of intraseasonal sea surface temperature (SST) anomalies and intraseasonal wind anomalies over the central Indian Ocean, and it preserves the mechanistic links among various dynamic and thermodynamic fields. Like a T junction, it controls the propagation direction of the intraseasonal variabilities (ISVs) originating in the western Indian Ocean. During the ISM, the CIO mode creates an environment favorable for the northward-propagating mesoscale variabilities. These results unveil the relation between the subseasonal monsoonal precipitation and the CIO mode in the ocean–atmosphere system in the Indian Ocean. The identification of the CIO mode deepens our understanding of the coupled monsoon system and brightens the prospects for better simulation and prediction of monsoonal precipitation in the affected countries.

1. Introduction

Precipitation during the Indian summer monsoon (ISM) is the lifeline for billions of people living on the rim of the Indian Ocean. The monsoonal precipitation is dominated by intraseasonal variabilities (ISVs), which are commonly known as the monsoon intraseasonal oscillation (MISO; Goswami 2005; Shukla 2014). For example, the variance of the intraseasonal precipitation accounts for about 60% of the total variance of precipitation over the Bay of Bengal (BoB). A comprehensive description of MISO is given by Annamalai and Slingo (2001), Waliser (2006), Annamalai and Sperber (2016), and Jones (2016). The MISO can be represented with a multivariate index that was established by Lee et al. (2013) and Suhas et al. (2013). The MISO is believed to be closely related to the northward-propagating ISVs. Yasunari (1980) was one of the pioneers to demonstrate that MISO was likely to originate from the ISVs over the equatorial Indian Ocean. Wang and Rui (1990) categorized the ISVs into three groups and found that the northward-propagating ISVs prevailed during boreal summer. Several mechanisms have been proposed for MISO. Webster (1983) hypothesized that the increased surface heat flux ahead of the convection over the continent destabilized the atmosphere,

Corresponding author e-mail: Lei Zhou, lzhou@sio.org.cn

DOI: 10.1175/JCLI-D-16-0347.1

leading to the northward propagation. However, in reality, the ISVs mainly propagate northward over the ocean, not over land. Wang and Xie (1997) argued that the apparent northward propagation of ISVs was actually a westward-tilting convection front, which emanated from the tropical Pacific as Rossby waves. This hypothesis was supported by the evidence that many northward-propagating ISVs coincided with the eastward-propagating ones. However, the independent northward-propagating ISVs, as categorized in Wang and Rui (1990), cannot be explained. Furthermore, the convective momentum transport (CMT; Kang et al. 2010) and the interaction between the perturbations and the background easterly shear (Jiang et al. 2004) were both found to be important for MISO. Using an idealized land–atmosphere coupled model, Bellon (2011) showed that the small heat capacity of the land greatly damped the ISVs over the Indian subcontinent, which could explain the small intraseasonal variance over land during ISM. Recently, the moisture effects during tropical convection has received much attention. For example, Kemball-Cook and Wang (2001) showed that a relation exists between the moist Kelvin–Rossby coupled waves and MISO; Abhik et al. (2013) argued that the atmospheric instability is attributable to the moisture convergence due to the low-level advection and subgrid eddies. Ocean–atmosphere interaction is another important mechanism since the warm sea surface temperature (SST) anomalies can cause moisture convergence in the atmospheric boundary layer, destabilizing the atmosphere to the north of convection (Kemball-Cook and Wang 2001; Vecchi and Harrison 2002; Fu and Wang 2004; Krishnan et al. 2011). In addition, the ocean is able to play an active role during MISO (Yano and McBride 1998; Zhou and Murtugudde 2014). In spite of the differences in details between the various mechanisms, one consensus is that the MISO stems from the tropical ISVs, which originally propagate eastward from the western equatorial Indian Ocean. It is still unclear what mechanism causes such tropical ISVs to take a ''left turn'' and propagate northward during ISM. This question is addressed in this study.

In addition, the relationship between the monsoonal precipitation and the intrinsic low-frequency modes in the coupled ocean–atmosphere system, mainly El Niño–Southern Oscillation (ENSO; e.g., Kumar et al. 1999; Krishnamurthy and Kirtman 2003; Gadgil et al. 2004; Kumar et al. 2006; Gill et al. 2015) and the Indian Ocean dipole/zonal mode (IODZM; e.g., Allan et al. 2001; Ashok et al. 2001; Abram et al. 2008; Sabeerali et al. 2012; Sabeerali et al. 2014), has been widely studied on the subseasonal-to-interannual and longer time scales. Although the variabilities on the intraseasonal time scale are pronounced during ISM, no mode is yet identified for the ISVs. In this study, a relation between the MISO and an intrinsic mode, the central Indian Ocean (CIO) mode, in the atmosphere–ocean system is established at intraseasonal time scales. Diagnostic results show that the CIO mode captures the mechanistic links among various dynamic and thermodynamic fields and plays an important role in influencing the propagation direction of the ISVs during the ISM.

The rest of this paper is organized as follows. The data are introduced in section 2. The phenomena and dynamics of the CIO mode are described in sections 3 and 4, respectively. The conclusions and discussion are presented in section 5.

2. Data

The atmospheric variables such as wind, precipitation, and relative humidity are obtained from the daily National Centers for Environmental Prediction (NCEP)–National Center for Atmospheric Research (NCAR) reanalysis (Kalnay et al. 1996), from 1982 to 2014. The atmospheric variables are also obtained from daily ERA-Interim data, the global atmospheric reanalysis produced by the European Centre for Medium-Range Weather Forecasts (ECMWF; Uppala et al. 2005) for the verification of the robustness of the results. The robustness of precipitation from a reanalysis product may be a concern. However, by comparing with the Tropical Rainfall Measuring Mission (TRMM) rainfall data, it can be shown that the NCEP–NCAR reanalysis has a reasonable rendition of both the total and the intraseasonal monsoonal rainfall. SST data are obtained from the NOAA ¼° daily Optimum Interpolation SST (Reynolds et al. 2007), from 1982 to 2014 and the outgoing longwave radiation (OLR) data are obtained from the NOAA satellite data (Liebmann and Smith 1996), from 1982 to 2013. All intraseasonal variabilities are obtained with a 20–100-day bandpass Butterworth filter.

3. Phenomenon of the central Indian Ocean mode

The mechanism of MISO is examined by contrasting the composites of two groups categorized with respect to the intraseasonal precipitation anomalies, which are the averages within 80°–95°E and 15°–24°N during the traditional ISM period from June to September (Fig. 1). One group consists of all intraseasonal precipitation anomalies that are larger than their mean (the mean of ISVs is almost zero; the solid black line in Fig. 1) plus their standard deviation (STD; the top dashed line in Fig. 1), which is referred to as the large-rainfall group hereafter, and the other group consists of all intraseasonal precipitation anomalies smaller than the mean

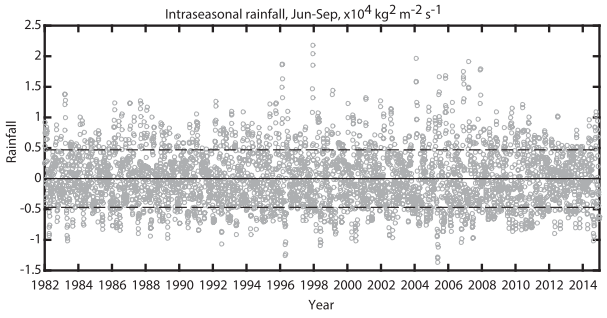

FIG. 1. Intraseasonal precipitation from the NCEP–NCAR reanalysis averaged over 80°–95°E and 15°–24°N during ISM (June–September). The black line is the mean of the intraseasonal precipitation and the two dashed lines denote the mean positive STD and mean negative STD of the intraseasonal precipitation.

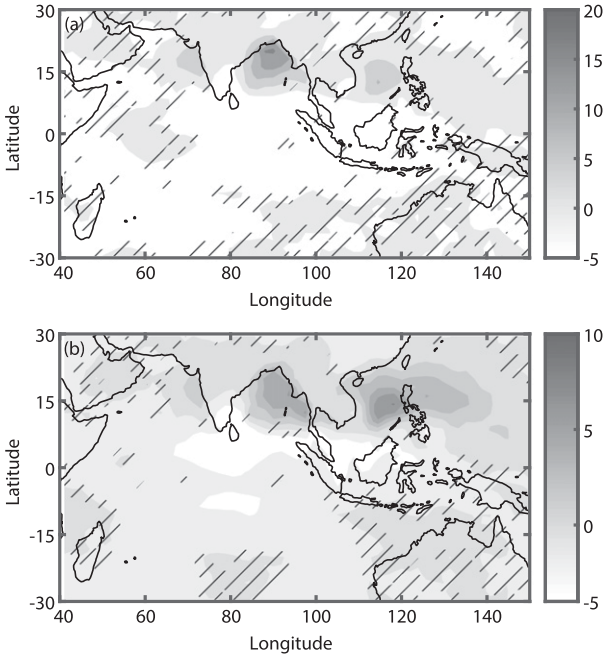

FIG. 2. (a) The differences in intraseasonal precipitation (10^{-5} kg^2 m^{-2} s^{-1}) between the large- and small-rainfall groups. (b) As in (a), but for the differences between the positive and negative phases of the CIO mode. The differences in the areas with no hatch lines are statistically significant at a 95% confidence level.

minus the STD (the bottom dashed line in Fig. 1), which is referred to as the small-rainfall group hereafter. The differences in the intraseasonal precipitation during ISM between the two groups are shown in Fig. 2a. The significant differences mainly occur over the northern BoB, where the monsoonal precipitation is pronounced. The differences in the intraseasonal SST anomalies and intraseasonal wind anomalies in the lower troposphere at 850 hPa between the two groups are shown in Fig. 3a. During the days with large intraseasonal precipitation, there are warm SST anomalies over the central Indian Ocean along the equator. The negative SST anomalies occur off the Somali coast and cross the Arabian Sea and BoB. For the days with small intraseasonal precipitation, the ISV patterns are largely opposite to what are shown in Fig. 3a (i.e., negative SST anomalies in the central Indian Ocean and positive SST anomalies crossing the Arabian Sea and BoB). Corresponding to these SST anomalies, there is an anticyclonic gyre in the lower troposphere, as shown with black vectors in Fig. 3a. This anticyclonic gyre is similar to the mean atmospheric general circulation during ISM (Webster et al. 1998; Goswami and Mohan 2001). However, there are fundamental differences in the physical mechanism. First, the two gyres are separated in time scales; the former is in the intraseasonal band, while the latter is in the seasonal band that provides a background state for the former. Second, the structures and dynamics of the air–sea interaction are different. Seasonal mean easterlies occur in the Southern Hemisphere along the isotherms on the edge of the warm pool over the eastern Indian Ocean, connecting to the Findlater jet (Schott and McCreary 2001) and contributing to the energy transfer from the Southern Hemisphere to the Northern Hemisphere during the ISM (Schott and McCreary 2001; Schneider et al. 2014). In contrast, as shown in Figs. 3b,c, the intraseasonal anticyclone is mainly attributable to the conservation of the potential vorticity (PV; Hoskins et al. 1985; Zhang and Ling 2012). Zhang and Ling (2012) showed that PV can represent the major properties of the ISVs. In the isobaric (pressure) coordinate, PV is defined as $\mathbf{P} = -g(f\mathbf{k} + \nabla \times \mathbf{V}) \cdot \nabla\theta$, where g is the gravitational acceleration; f is the Coriolis parameter; $\mathbf{V} = u\mathbf{i} + v\mathbf{j} + \omega\mathbf{k}$, where u, v, and ω are the eastward, northward, and vertical pressure velocities, respectively; $\mathbf{i}$, $\mathbf{j}$, and $\mathbf{k}$ are the unit vectors pointing to the east, north, and vertical, respectively; θ is the air potential temperature; and $\nabla = \mathbf{i}\partial/\partial x + \mathbf{j}\partial/\partial y + \mathbf{k}\partial/\partial p$. Usually, since the vertical component of $\mathbf{P}$ dominates, only the vertical component of PV is used in this study, which is calculated as $-g(f+\zeta)\partial\theta/\partial p$, where $\zeta = \partial v/\partial x + \partial u/\partial y$ is the relative vorticity of the air. PV is generally conserved unless it is modified by diabatic heating or friction. Given the PV conservation, the distribution of PV on an isobaric surface can diagnostically deduce most dynamical fields, such as the horizontal wind anomalies (Hoskins et al. 1985). In the lower troposphere (Fig. 3b), the easterly wind anomalies enhanced by the underlying warm SST anomalies along the equator turn northward around 70°E, roughly following the contours of PV. In the northern BoB, there is a positive PV center, which is consistent with the cyclone there. In the upper troposphere at 300 hPa (Fig. 3c), the

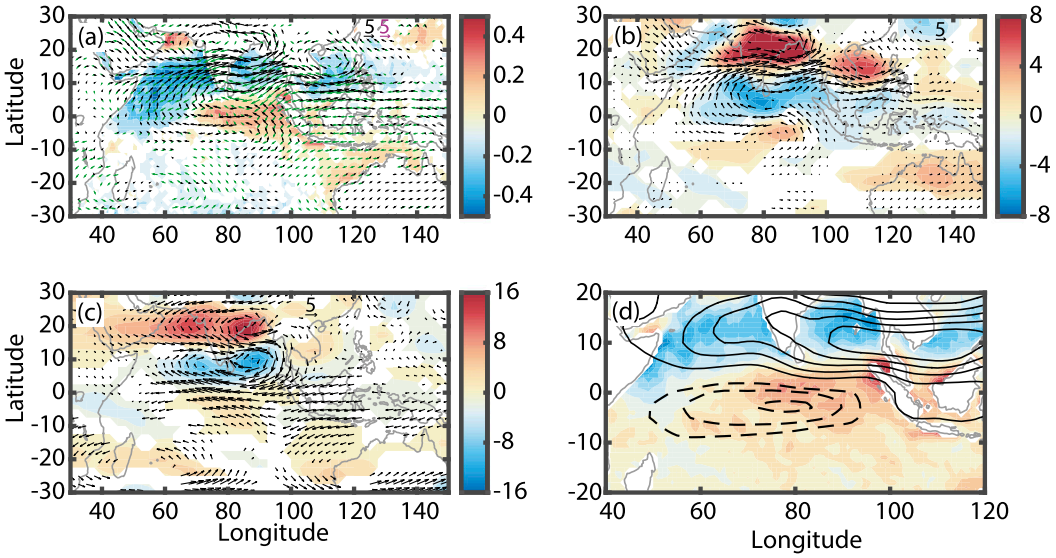

FIG. 3. (a) The differences between the large- and small-rainfall groups in intraseasonal SST anomalies (color shading; °C), intraseasonal wind anomalies at 850 hPa (black vectors; m s^{-1}), and vertical wind shear (green vectors; kg m^{-2} s^{-1}). (b) The differences in intraseasonal PV anomalies at 850 hPa (color shading; 10^{-2} PVU; 1 PVU = 10^{-6} m^2 K s^{-1} kg^{-1}) and intraseasonal wind anomalies at 850 hPa (black vectors; m s^{-1}). (c) As in (b), but for the upper troposphere at 300 hPa. (d) The pattern of the positive CIO mode. Reddish (bluish) color denotes the positive (negative) node of the SST mode. Solid (dashed) contours denote the positive (negative) node of the zonal wind mode. All color shading and vectors shown in (a)–(c) are significant at a 95% confidence level.

anticyclone (cyclone) in the southern (northern) BoB is coherently constrained by the conservation of PV since the diabatic heating and friction, which are the major source and sink of PV, are also small in the upper troposphere.

The above structures associated with MISO represent an intrinsic mode in the Indian Ocean, which incorporates both the atmospheric and oceanic properties. The empirical orthogonal function (EOF) analysis is conducted in the Indian Ocean to isolate this intrinsic mode. A combined field of the daily intraseasonal SST data and daily intraseasonal zonal winds at 850 hPa from 1982 to 2014 is employed for the EOF analysis. The domain is from 40° to 120°E and from 20°N to 20°S, which is what is commonly used (e.g., Murtugudde and Busalacchi 1999; Saji et al. 1999; Murtugudde et al. 2000). Each field is normalized by subtracting its regional mean and then divided by its regional variance within the above domain before doing the EOF analysis, so that the SST and winds can be compared and combined. It has been well known that the first EOF mode of the SST anomalies in the Indian Ocean is the basin mode (Yang et al. 2007, 2009) and the second EOF mode is the IODZM (Saji et al. 1999; Li et al. 2003; Saji and Yamagata 2003; Annamalai and Murtugudde 2004), which has been widely studied since its discovery. The EOF analysis was also conducted using the ISVs in OLR, zonal winds in the lower troposphere, and the multivariate fields (Goswami and Mohan 2001; Wheeler and Hendon 2004; Lee et al. 2013; Suhas et al. 2013; Shukla 2014). As shown in Fig. 3d, the atmospheric and oceanic features of the MISO are captured by the first combined EOF mode of intraseasonal SST anomalies and intraseasonal zonal winds at 850 hPa, which explains 13.6% of the total variance. The positive SST node of the combined EOF mode captures warm intraseasonal SST anomalies along the central Indian Ocean. Correspondingly, the negative wind node denoting the equatorial easterlies and the positive wind node denoting the westerlies from the Arabian Sea to the South China Sea (SCS) indicate an anticyclonic gyre between the tropics and subtropics, which is consistent with the low-level winds in Fig. 3a (black vectors). Hereafter, we refer to the first EOF mode shown in Fig. 3d as the CIO mode, since the key feature and a major node of this mode is the consistent structure between the intraseasonal dynamic and thermodynamic fields over the central Indian Ocean. The positive (negative) CIO mode is defined when there are pronounced warm (cool) SST anomalies and an anticyclone (cyclone) over the central Indian Ocean and the first principal component (PC1) is significantly positive (negative). The differences in composite intraseasonal precipitation between the positive CIO mode and the negative CIO mode are shown in

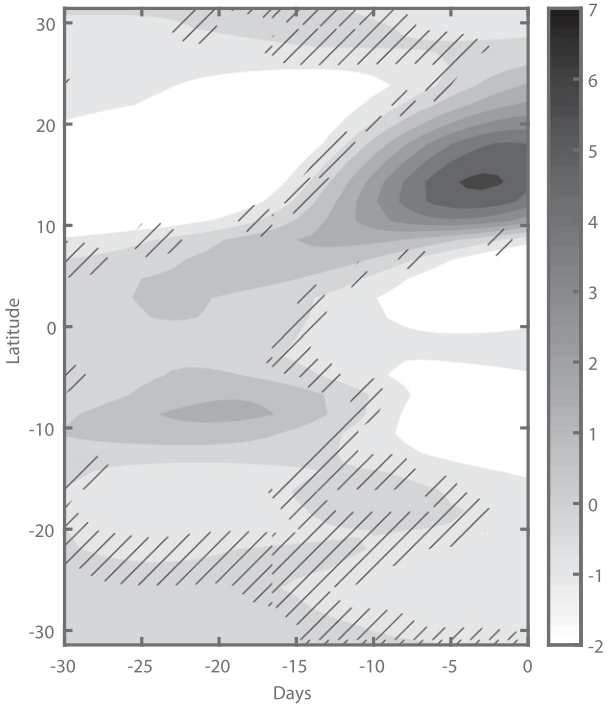

FIG. 4. Hovmöller diagram of the differences in composite intraseasonal precipitation anomalies between the positive and negative phases of the CIO mode. The intraseasonal precipitation is averaged between 80° and 100°E (10^{-5} kg^2 m^{-2} s^{-1}). Day 0 is the day when PC1 reaches its local maximum (minimum) for the positive (negative) CIO mode, and negative days indicate the days before day 0. The differences in the areas with no hatch lines are statistically significant at a 95% confidence level.

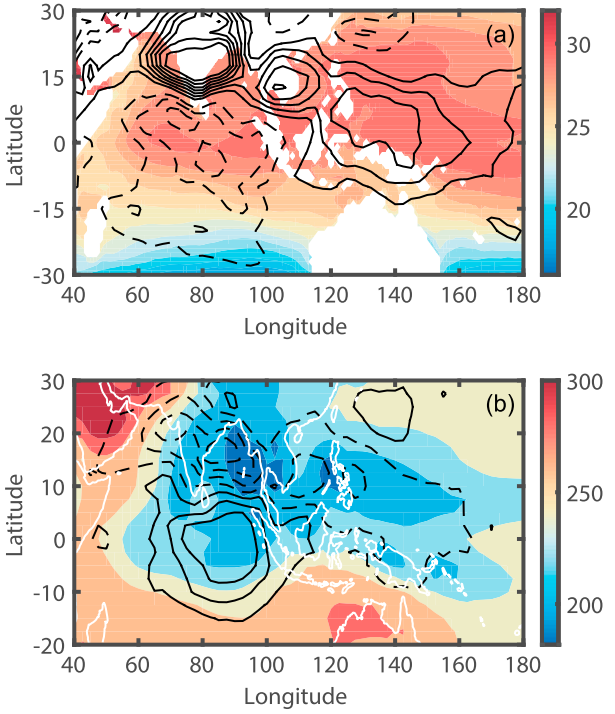

FIG. 5. (a) Mean SST (°C) during the ISM (color shading) and differences in intraseasonal specific humidity at 500 hPa between the large-rainfall group and the small-rainfall group (contours). The contours start from $\pm 10^{-4}$ kg kg^{-1} and the interval is 10^{-4} kg kg^{-1}. (b) Mean OLR (color shading; W m^{-2}) during the ISM and differences in the intraseasonal OLR anomalies between the large-rainfall group and the small-rainfall group (contours). The contours start from ± 5 W m^{-2} and the interval is 10 W m^{-1}. Solid (dashed) contours denote positive (negative) anomalies. All differences shown with the contours are statistically significant at a 95% confidence level.

Fig. 2b, which are similar to the differences between the large-rainfall and the small-rainfall groups shown in Fig. 2a. The northward propagation associated with the CIO mode is shown with the differences in the intraseasonal precipitation between the positive and the negative CIO mode phases (Fig. 4). Day 0 is the day when PC1 reaches its local maximum (minimum) for the positive (negative) CIO mode, and negative days in Fig. 4 indicate the days before day 0. In addition, the composites of intraseasonal SST anomalies and intraseasonal wind anomalies for the positive (negative) CIO mode are also similar to the ones for the large (small) rainfall group (not shown). Overall, the properties associated with the CIO mode well capture the main features of the MISO.

4. Dynamics of the central Indian Ocean mode

The downdraft over the central Indian Ocean associated with deep convection over the western Pacific warm pool is the trigger for the intrinsic CIO mode. The clear sky over the central Indian Ocean due to the downdraft increases the incident solar radiation at the sea surface, leading to warm SST anomalies (i.e., the positive CIO mode). During the ISM, the warm pool (where the SSTs are larger than 28°C) extends from the equator to 20°N over the western Pacific Ocean (Fig. 5a). Correspondingly, the mean ITCZ centers around 10°N (Fig. 5b). However, the synoptic convection does not follow the mean warm SST exactly, since deep convection is bounded by the large-scale dynamical subsidence (Takayabu et al. 2010). The differences in midtropospheric intraseasonal specific humidity and the differences in intraseasonal OLR anomalies, both of which are good indicators of tropical convection between the large-rainfall group and small-rainfall group, straddle the equator (Fig. 5). The differences in the intraseasonal zonal and vertical momentum between the two groups are shown in Fig. 6. Because of the air density ρ differences in the upper and lower troposphere, the momentum (ρu, $\rho\omega$) rather than (u, ω), where u and ω are the zonal and vertical velocities, is used in Fig. 6. Deep convection over the western Pacific is stronger for

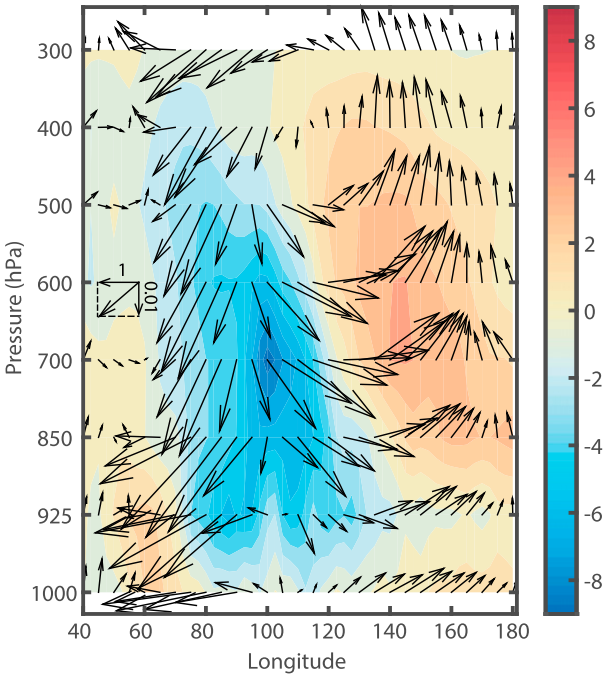

FIG. 6. Differences of specific humidity (color shading; 10^{-4} kg kg^{-1}) and zonal momentum ρu (kg m^{-2} s^{-1}) and vertical momentum $\rho\omega$ (ω is the vertical pressure velocity; kg Pa m^{-3} s^{-1}).

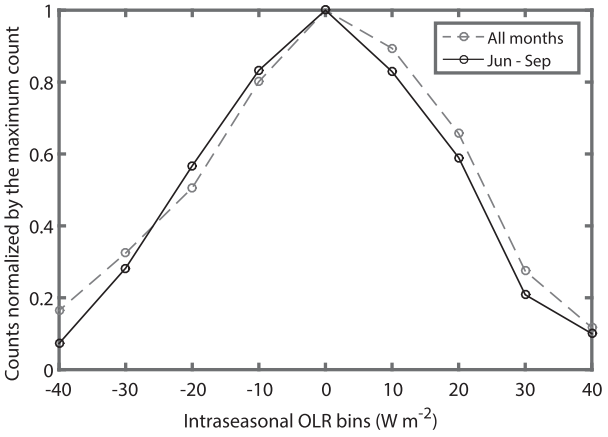

FIG. 7. Distribution of intraseasonal OLR anomalies averaged over 5°N–5°S, 70°–80°E, normalized by the maximum counts in the distribution. The gray dashed curve is the distribution for all months from 1982 to 2013, and the black solid curve is the distribution for ISM from June to September.

the large-rainfall group. Correspondingly, the downdraft occurs from central to eastern Indian Ocean between 70° and 120°E. The variability in vertical motion can be clearly detected from the vertical profile of specific humidity, which is critical for atmospheric instability and tropical convection. As a result, for the positive CIO mode, specific humidity increases in the midtroposphere over the tropical western Pacific because of the local enhanced deep convection, while the central Indian Ocean becomes dry because of the downdraft associated with this deep convection. Note that the zonal convection cell shown in Fig. 6 is separated from the well-known Walker cell on both temporal and spatial scales. The convection cell associated with the subseasonal CIO mode is significantly smaller in its zonal extent than the Walker cell, which is closely related to ENSO, IODZM, and the Indo-Pacific tripole (Chen and Cane 2008; Chen 2011; Lian et al. 2014) that dominate the interannual variability over the whole globe. The multiscale nature of the tropical convection system has been explored before (Hendon and Liebmann 1994; Biello and Majda 2005; Tulich and Mapes 2008; Kikuchi and Wang 2010), but here we capture for the first time the intrinsic mode that steers the poleward propagation originating in the Indian Ocean on intraseasonal time scales. The updraft branch of Walker circulation occurs over the Indo-Pacific warm pool ranging from the eastern Indian Ocean to the western Pacific Ocean (roughly from 90° to 160°E, albeit a little weaker over the Maritime Continent) and the downdraft on the Indian Ocean side mainly occurs over the western Indian Ocean to the west of 60°E, which is largely consistent with the mean SST distribution shown in Fig. 5a. In contrast, the convection cell associated with the CIO mode (Fig. 6) is narrower and is mainly consistent with the synoptic convection from the western Pacific to the central Indian Ocean. In addition, the convection cell with the CIO mode is very much local and does not have a branch over the Pacific Ocean as the Walker cell does.

Over the central tropical Indian Ocean, the mean SSTs during ISM are actually slightly cooler than the adjoining areas (Fig. 5a). However, the intraseasonal warm SST anomalies are pronounced during the positive CIO mode and create a favorable environment for MISO. The different relative SST anomalies between the central Indian Ocean and the adjacent regions indicate a separation between the subseasonal scale and the seasonal scale, which is probably due to the ocean–atmosphere interaction dynamics associated with the CIO mode. In reality, the origin of ISVs usually resides in the western Indian Ocean (Seo and Kim 2003; Zhao et al. 2013). There is a year-around shallow convection and a moderate increase of humidity in the lower troposphere, which is critical for the initialization of the Madden–Julian oscillation (MJO), which is the major component of eastward-propagating ISVs in the tropics (Zhang 2005). Convection (denoted with the negative OLR anomalies) has a very similar statistical distribution as shown in Fig. 7, which indicates that convection over the western Indian Ocean can always occur following a

very similar statistical distribution, although the mechanism for the generation of convection over the western Indian Ocean is still debated (Kemball-Cook and Weare 2001; Matthews 2008; Straub 2013). In boreal winter, the ISVs (mainly MJO) mostly propagate eastward across the central and eastern Indian Ocean. But during ISM, most ISVs veer northward, which is attributed to the atmospheric circulation modified by the CIO mode. Although the downdraft leads to anticyclones in both the upper and the lower troposphere, the wind anomalies actually enhance the easterly vertical wind shear. Usually, the vertical wind shear is calculated using the wind in the upper atmosphere minus the wind in the lower atmosphere. The easterly wind shear is favorable for the northward propagation of ISV via the CMT (Kang et al. 2010). The downdraft over the central Indian Ocean brings easterly momentum from the upper troposphere to the lower troposphere. Hence, an eastward Coriolis force is required to balance the westward CMT forcing. As a result, a secondary meridional convection cell is induced, with a northward (southward) branch in the lower (upper) troposphere (see Fig. 3 in Kang et al. 2010). Similarly, using a two-layer idealized model, Jiang et al. (2004) showed that the barotropic vorticity and the baroclinic divergence are coupled by the easterly vertical wind shear. The baroclinic divergence, which coincides with the convection center, can induce a positive barotropic vorticity to the north, which consequently enhances the convergence in the planetary boundary layer (PBL) and increases the moisture transport from PBL to the free troposphere to the north of convection, inducing the northward propagation of the ISVs. According to both mechanisms, the mesoscale atmospheric circulation modified by the warm SST anomalies shifts the ISVs originating in the western Indian Ocean to the north, leading to MISO and the supply of momentum and moisture for the onset and heavy precipitation during ISM (Fu et al. 2003; Zhou and Murtugudde 2014). To show the consistency between the warm SST anomalies associated with the positive CIO mode and the precipitation over BoB, we define a convection event over the western Indian Ocean when the consecutive days with intraseasonal OLR anomalies lower than $-25\,\mathrm{W\,m^{-2}}$ last for 10 days with fewer than 3 break days (the day with an intraseasonal OLR anomaly larger than $-25\,\mathrm{W\,m^{-2}}$). The scatterplot of the intraseasonal SST in the central Indian Ocean (averaged between 5°N and 5°S and between 80° and 90°E) and precipitation anomalies over the northern BoB (averaged between 15° and 24°N and between 85° and 95°E) after the convection events are shown in Fig. 8a. All anomalies in Fig. 8a are averaged between

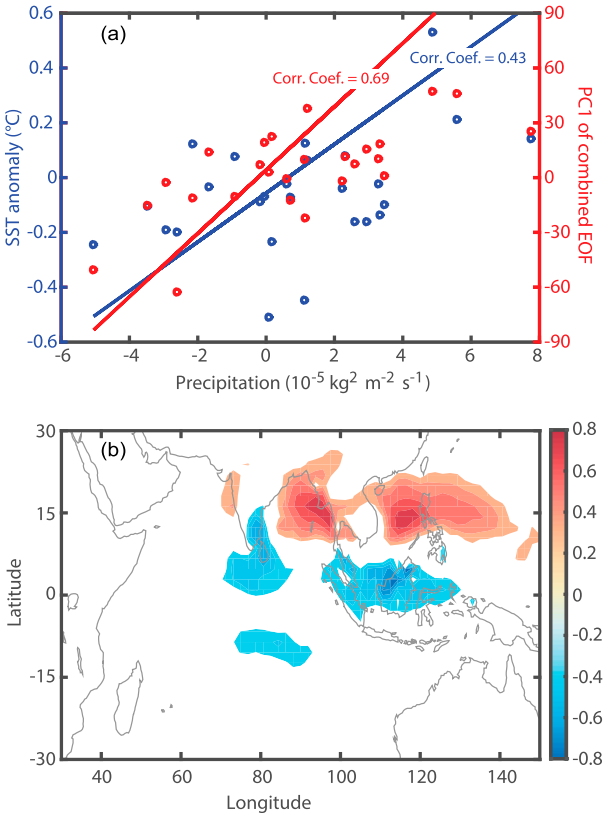

FIG. 8. (a) The scatterplot of the intraseasonal SST anomalies (averaged over 5°N–5°S, 80°–90°E) and the intraseasonal precipitation anomalies (averaged over 15°–24°N, 85°–95°E) for convection events over the western Indian Ocean. All anomalies are averaged between 5 and 10 days after the central day of the convection events, when the intraseasonal OLR anomalies over western Indian Ocean reach their minimum. (b) Correlation coefficients between PC1 of the CIO mode and intraseasonal precipitation during ISM, which are statistically significant at a 95% confidence level. The effective sample size is adjusted following Bretherton et al. (1999) so that the influence of bandpass filtering on the significance test of the correlation coefficient is removed.

5 and 10 days after the central day of the convection events, which is a reasonable period for the ISVs propagating from the western Indian Ocean to the central Indian Ocean. The correlation coefficient is 0.43 (statistically significant at a 97% confidence level), which indicates that warm intraseasonal SST anomalies of the positive CIO mode are necessary to steer the ISVs originating from the western Indian Ocean to the north and lead to heavy monsoonal rainfall over BoB. The linear relation is robust and is not sensitive to the time period used for the averaging. Note that the effective sample size (ESS) is reduced by the bandpass filtering. When performing the significance test on the correlation coefficient, the ESS is adjusted following Bretherton et al. (1999), so that the influence of high autocorrelation of each bandpass-filtered time series is

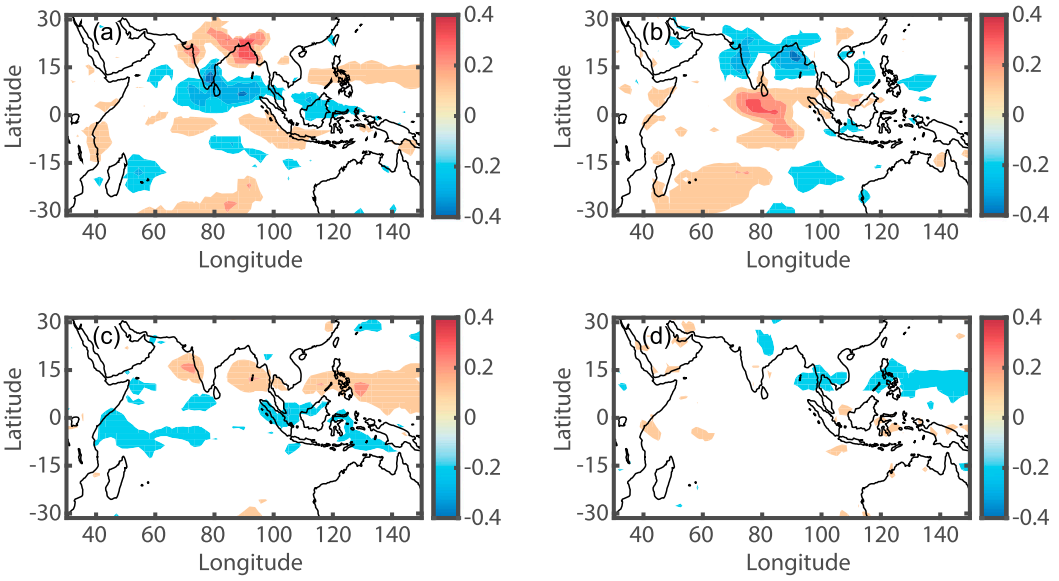

FIG. 9. The correlation coefficients between intraseasonal precipitation and (a) intraseasonal SST anomalies averaged over the central Indian Ocean (5°N–5°S, 80°–90°E), (b) DMI, (c) TNI, and (d) Niño-3.4 index. To retain the ISVs in all indices, daily data are used for the calculations and no smoothing in time is applied. All correlation coefficients are smaller than 0.4, which are much less than the ones shown in Fig. 8b. All shown coefficients are statistically significant at a 95% confidence level.

removed. The CIO mode represents the consistent structure between the dynamic and thermodynamic fields in the ocean and the atmosphere. Thus, it has a better linear correlation (the correlation coefficient is 0.69 at a 99% confidence level) with the monsoonal precipitation as shown in Fig. 8b. In addition, the correlation coefficients between the principal component of CIO mode and the intraseasonal monsoonal precipitation can reach a maximum of 0.8 over the northern BoB (Fig. 8b), which is much larger than the monsoon correlations with the common indices for ENSO and IODZM (Fig. 9). ENSO is denoted with the trans-Niño index (TNI; Trenberth 1997; Trenberth and Stepaniak 2001; Fig. 9c) and Niño-3.4 index (Fig. 9d). IODZM is denoted with the dipole model index (DMI; Saji et al. 1999; Fig. 9b). Usually, the indices for ENSO and IODZM are made with monthly data. But, in order to retain the ISVs in all indices, daily data are used for the calculations and no smoothing in time is applied in this study. Recently, considerable efforts have been made to improve the prediction of the ISM rainfall (e.g., Webster and Hoyos 2004; Abhilash et al. 2013). Although some successes have been achieved, the predictability is still very limited, partly as a result of the weak correlations between the ISM monsoon rainfall and the traditional weather and climate indices (Webster et al. 1998; Wang et al. 2009, 2015). Thus, the large correlations of the CIO mode imply a potential advance in predictive understanding of MISO as well.

The transit between the positive and negative CIO mode occurs as a result of the ocean–atmosphere interactions over the eastern Indian Ocean. The composite Hovmöller diagram of intraseasonal SST anomalies for the positive CIO mode is shown in Fig. 10. The intraseasonal SST anomalies are averaged between 5°N and 5°S. Day 0 is the day with heavy precipitation (i.e., the day when the intraseasonal rainfall is larger than the mean plus the STD). There are 644 such days from 1982 to 2014. Warm SST anomalies occur about 5 days before the heavy precipitation over BoB (Xi et al. 2015). The warm SST anomalies continue to increase since the easterly winds, the equatorial arm of the anticyclone (black vectors in Fig. 3a), continue to transport warm water from the east to the west. In addition, the westerly mean winds during the ISM are weakened by the easterly anomalies, which reduce the latent heat flux and contribute to the warm SST anomalies. Note that Fig. 10 shows the average in the deep tropics between 5°S and 5°N. Along the equator, usually the eastward-propagating Kelvin waves dominate (Valsala 2008; Zhou and Murtugudde 2010). However, the westward propagation is obvious in Fig. 10, which is probably driven by the easterly wind anomalies. Around day 10, negative SST anomalies begin to occur off Sumatra, which is likely to be generated by the coastal upwelling. Then, the cold water is brought to the west also by the easterlies to finally erase the warm anomalies over the central Indian Ocean. Such negative feedback is likely to

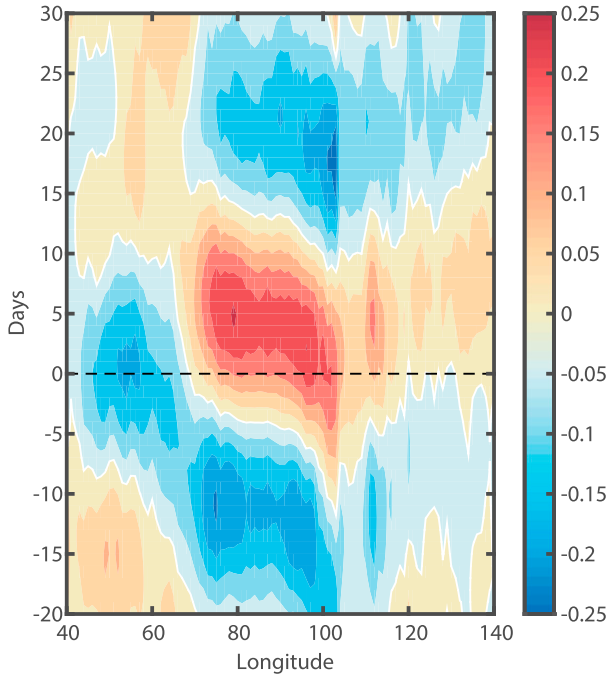

FIG. 10. Hovmöller diagram of intraseasonal SST anomalies (°C) in the tropics for the positive CIO mode. Intraseasonal SST anomalies are averaged over 5°N–5°S. Day 0 is the day with heavy precipitation (i.e., the day when the intraseasonal rainfall is larger than the mean plus the STD). There are 644 such days from 1982 to 2014. Negative (positive) days are before (after) day 0.

control the life cycle of the CIO mode, which depends on the background state. If there is a relatively thick layer of warm water in some years off Sumatra, it will take relatively longer for the dissipation of warm SSTs and the CIO phase transition to occur. On the contrary, if the warm water layer off Sumatra is thin, it will be eroded faster. This indicates an irregularity of the CIO mode and the low-frequency variability (such as the interannual variability) of the CIO mode. Moreover, the strong ocean mixing of surface and subsurface waters over the central Indian Ocean may also play a role during the CIO mode, as shown with observations by Pujiana et al. (2015). Most present-day oceanic reanalysis products are not good enough to capture the ISVs in the ocean interior (Zhang et al. 2016). Thus, a solid conclusion about the relation between the oceanic processes and the CIO mode requires more observations and detailed analysis in the future. In addition, the eastward deepening of the thermocline in the Indian Ocean, which is quite unlike the equatorial Pacific and Atlantic Oceans, is well known (Murtugudde and Busalacchi 1999). The interannual variability of the thermocline is of interest in the context of IODZM, but interactions of these lower frequencies with the intraseasonal time scale can occur through the CIO mode. This would offer a new avenue to investigate the interannual and lower-frequency variabilities of MISO and the monsoon itself, likely including the pathways for IODZM and ENSO influences on the monsoon.

5. Conclusions and discussion

In this study, we find an intrinsic mode in the Indian Ocean, the CIO mode, which is closely related to the heavy precipitation during the Indian summer monsoon season. The warm intraseasonal SST anomalies and the associated anticyclone are the key features of the positive CIO mode, which modifies the atmospheric circulation over the Indo-Pacific region and creates a favorable environment for MISO. The CIO mode is like a T junction that controls whether the ISVs can propagate northward into BoB. The entire sequence of processes is summarized in Fig. 11. The CIO mode has a high simultaneous correlation with MISO during ISM, which is expected to contribute to improve the predictive understanding of MISO. It is necessary to make comprehensive evaluations of the CIO mode contribution to the MISO prediction in the future. In addition, the oceanic responses and feedbacks to the CIO mode require further study, probably using an ocean–atmosphere coupled model.

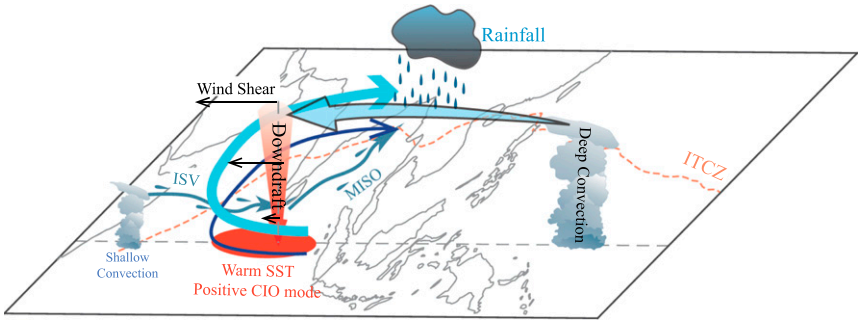

FIG. 11. Sketch for the positive CIO mode and the associated atmospheric and oceanic anomalies.

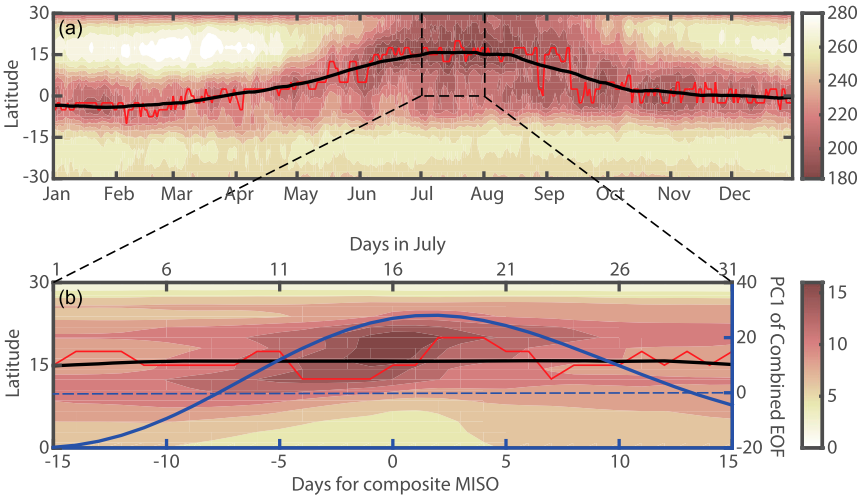

FIG. 12. (a) The mean daily OLR ($W\,m^{-2}$) averaged from 1982 to 2013 between 80° and 100°E. The red line marks the latitude with the minimum OLR for each day. The black line denotes the ITCZ, which is obtained with a 60-day running mean of the red line so that the ISVs are largely removed. (b) The red line and the black line are as in (a), but zoomed in during July. The color shading represents the northward-propagating MISO with the composite precipitation of the large-rainfall group (10^{-5} $kg\,m^{-2}\,s^{-1}$). Maximum precipitation over the northern BoB occurs on day 0 (lower horizontal axis). Negative days are before day 0, and positive days are after day 0. The blue line (vertical axis on the right) is the principal component of the CIO mode (i.e., the first combined EOF mode).

The CIO mode is a piece of the puzzle in the regional characteristics of the global ITCZ variability. On annual and longer time scales (including the geological epochs), the ITCZ usually locates in the warm hemisphere, maintaining the atmospheric energy balance (Schneider et al. 2014). On seasonal time scale, the energetic constraint is still operational. However, the jump of the ITCZ from the Southern Hemisphere to the Northern Hemisphere during ISM is an exception (Fig. 12a), and several mechanisms have been proposed to address this sudden migration (Webster et al. 1998; Chao and Chen 2001; Bordoni and Schneider 2008; Boos and Kuang 2010; Wu et al. 2012). On the subseasonal time scale, the seasonal mean position of ITCZ does not change much and becomes the background state (black line in Fig. 12b). The CIO mode (blue line in Fig. 12b) leads to the northward-propagating MISO (color shading in Fig. 12b), which can overshoot the seasonal mean ITCZ, transferring moisture and momentum to far-northern locations. In the multiscale but ''seamless'' climate system, the CIO mode is certainly influenced by the background states, such as the ITCZ, convection over the Pacific warm pool, and ENSO, and it may also have feedbacks to the background state. In a multiscale system, the coexistence of the various spatiotemporal scales cannot always be neatly deconvolved, but the existence of the CIO mode points to its role in this complex multiscale system. Its scale selection and its relation to the other members of this important MJO–monsoon–ENSO system require further studies. Nonetheless, the phenology and mechanism of CIO mode we report here are advancements in the process understanding of the monsoon intraseasonal variability and should eventually lead to predictive understanding as well with further analysis of the CIO mode and its interactions with and feedbacks to the large-scale and lower-frequency modes of coupled ocean–atmosphere interactions.

Acknowledgments. This work is supported by grants from the National Natural Science Foundation of China (41376034, 41321004, and 41690121), the National Basic Research Program (2013CB430302), and the IPOVAR Project (GASI-IPOVAI-01-02 and GASI-IPOVAI-02). RM gratefully acknowledges the CYGNSS grant from NASA and the National Monsoon Mission funds for partial support.

REFERENCES

Abhik, S., M. Halder, P. Mukhopadhyay, X. Jiang, and B. N. Goswami, 2013: A possible new mechanism for northward propagation of boreal summer intraseasonal oscillations based on TRMM and MERRA reanalysis. *Climate Dyn.*, **40**, 1611–1624, doi:10.1007/s00382-012-1425-x.

Abhilash, S., A. K. Sahai, S. Pattnaik, and S. De, 2013: Predictability during active break phases of Indian summer monsoon in an ensemble prediction system using climate

forecast system. *J. Atmos. Sol. Terr. Phys.*, **100–101**, 13–23, doi:10.1016/j.jastp.2013.03.017.

Abram, N. J., M. K. Gagan, J. E. Cole, W. S. Hantoro, and M. Mudelsee, 2008: Recent intensification of tropical climate variability in the Indian Ocean. *Nat. Geosci.*, **1**, 849–853, doi:10.1038/ngeo357.

Allan, R. J., and Coauthors, 2001: Is there an Indian Ocean dipole and is it independent of the El Niño-Southern Oscillation? *CLIVAR Exchanges*, No. 6, International CLIVAR Project Office, Southampton, United Kingdom, 18–22.

Annamalai, H., and M. J. Slingo, 2001: Active/break cycles: Diagnosis of the intraseasonal variability of the Asian summer monsoon. *Climate Dyn.*, **18**, 85–102, doi:10.1007/s003820100161.

——, and R. Murtugudde, 2004: Role of the Indian Ocean in regional climate variability. *Earth's Climate*, *Geophys. Monogr.*, Vol. 147, Amer. Geophys. Union, 213–246.

——, and K. R. Sperber, 2016: South Asian summer monsoon variability in a changing climate. *The Monsoons and Climate Change: Observations and Modeling*, V. L. M. de Carvalho and C. Jones, Eds., Springer, 25–46.

Ashok, K., Z. Guan, and T. Yamagata, 2001: Impact of the Indian Ocean dipole on the relationship between the Indian monsoon rainfall and ENSO. *Geophys. Res. Lett.*, **28**, 4499–4502, doi:10.1029/2001GL013294.

Bellon, G., 2011: Monsoon intraseasonal oscillation and land–atmosphere interaction in an idealized model. *Climate Dyn.*, **37**, 1081–1096, doi:10.1007/s00382-010-0893-0.

Biello, J. A., and A. J. Majda, 2005: A new multiscale model for the Madden–Julian oscillation. *J. Atmos. Sci.*, **62**, 1694–1721, doi:10.1175/JAS3455.1.

Boos, W. R., and Z. Kuang, 2010: Dominant control of the South Asian monsoon by orographic insulation versus plateau heating. *Nature*, **463**, 218–222, doi:10.1038/nature08707.

Bordoni, S., and T. Schneider, 2008: Monsoons as eddy-mediated regime transitions of the tropical overturning circulation. *Nat. Geosci.*, **1**, 515–519, doi:10.1038/ngeo248.

Bretherton, C. S., M. Widmann, V. P. Dymnikov, J. M. Wallace, and I. Bladé, 1999: The effective number of spatial degrees of freedom of a time-varying field. *J. Climate*, **12**, 1990–2009, doi:10.1175/1520-0442(1999)012<1990:TENOSD>2.0.CO;2.

Chao, W. C., and B. Chen, 2001: The origin of monsoons. *J. Atmos. Sci.*, **58**, 3497–3507, doi:10.1175/1520-0469(2001)058<3497:TOOM>2.0.CO;2.

Chen, D., 2011: Indo-Pacific tripole: An intrinsic mode of tropical climate variability. *Advances in Geosciences*, K. Satake and J. Gan, Eds., Vol. 24, World Scientific, 1–18.

——, and M. A. Cane, 2008: El Niño prediction and predictability. *J. Comput. Phys.*, **227**, 3625–3640, doi:10.1016/j.jcp.2007.05.014.

Fu, X. H., and B. Wang, 2004: Differences of boreal summer intraseasonal oscillations simulated in an atmosphere–ocean coupled model and an atmosphere-only model. *J. Climate*, **17**, 1263–1271, doi:10.1175/1520-0442(2004)017<1263:DOBSIO>2.0.CO;2.

——, ——, T. Li, and J. P. McCreary, 2003: Coupling between northward-propagating, intraseasonal oscillations and sea surface temperature in the Indian Ocean. *J. Atmos. Sci.*, **60**, 1733–1753, doi:10.1175/1520-0469(2003)060<1733:CBNIOA>2.0.CO;2.

Gadgil, S., P. N. Vinayachandran, P. A. Francis, and S. Gadgil, 2004: Extremes of the Indian summer monsoon rainfall, ENSO and equatorial Indian Ocean oscillation. *Geophys. Res. Lett.*, **31**, L12213, doi:10.1029/2004GL019733.

Gill, E. C., B. Rajagopalan, and P. Molnar, 2015: Subseasonal variations in spatial signatures of ENSO on the Indian summer monsoon from 1901 to 2009. *J. Geophys. Res. Atmos.*, **120**, 8165–8185, doi:10.1002/2015JD023184.

Goswami, B. N., 2005: South Asian monsoon. *Intraseasonal Variability in the Atmosphere–Ocean Climate System*, K. Lau and D. Waliser, Eds., Springer, 19–61.

——, and R. S. A. Mohan, 2001: Intraseasonal oscillations and interannual variability of the Indian summer monsoon. *J. Climate*, **14**, 1180–1198, doi:10.1175/1520-0442(2001)014<1180:IOAIVO>2.0.CO;2.

Hendon, H. H., and B. Liebmann, 1994: Organization of convection within the Madden-Julian oscillation. *J. Geophys. Res.*, **99**, 8073–8083, doi:10.1029/94JD00045.

Hoskins, B. J., M. E. McIntyre, and A. W. Robertson, 1985: On the use and significance of isentropic potential vorticity maps. *Quart. J. Roy. Meteor. Soc.*, **111**, 877–946, doi:10.1002/qj.49711147002.

Jiang, X. N., T. Li, and B. Wang, 2004: Structures and mechanisms of the northward propagating boreal summer intraseasonal oscillation. *J. Climate*, **17**, 1022–1039, doi:10.1175/1520-0442(2004)017<1022:SAMOTN>2.0.CO;2.

Jones, C., 2016: The Madden–Julian oscillation and the monsoons. *The Monsoons and Climate Change: Observations and Modeling*, V. L. M. de Carvalho and C. Jones, Eds., Springer International Publishing, 207–224.

Kalnay, E., and Coauthors, 1996: The NCEP/NCAR 40-Year Reanalysis Project. *Bull. Amer. Meteor. Soc.*, **77**, 437–471, doi:10.1175/1520-0477(1996)077<0437:TNYRP>2.0.CO;2.

Kang, I.-S., D. Kim, and J.-S. Kug, 2010: Mechanism for northward propagation of boreal summer intraseasonal oscillation: Convective momentum transport. *Geophys. Res. Lett.*, **37**, L24804, doi:10.1029/2010GL045072.

Kemball-Cook, S., and B. Wang, 2001: Equatorial waves and air–sea interaction in the boreal summer intraseasonal oscillation. *J. Climate*, **14**, 2923–2942, doi:10.1175/1520-0442(2001)014<2923:EWAASI>2.0.CO;2.

——, and B. C. Weare, 2001: The onset of convection in the Madden–Julian oscillation. *J. Climate*, **14**, 780–793, doi:10.1175/1520-0442(2001)014<0780:TOOCIT>2.0.CO;2.

Kikuchi, K., and B. Wang, 2010: Spatiotemporal wavelet transform and the multiscale behavior of the Madden–Julian oscillation. *J. Climate*, **23**, 3814–3834, doi:10.1175/2010JCLI2693.1.

Krishnamurthy, V., and B. P. Kirtman, 2003: Variability of the Indian Ocean: Relation to monsoon and ENSO. *Quart. J. Roy. Meteor. Soc.*, **129**, 1623–1646, doi:10.1256/qj.01.166.

Krishnan, R., S. Sundaram, P. Swapna, V. Kumar, D. C. Ayantika, and M. Mujumdar, 2011: The crucial role of ocean–atmosphere coupling on the Indian monsoon anomalous response during dipole events. *Climate Dyn.*, **37**, 1–17, doi:10.1007/s00382-010-0830-2.

Kumar, K. K., B. Rajagopalan, and M. A. Cane, 1999: On the weakening relationship between the Indian monsoon and ENSO. *Science*, **284**, 2156–2159, doi:10.1126/science.284.5423.2156.

——, ——, M. Hoerling, G. Bates, and M. Cane, 2006: Unraveling the mystery of Indian monsoon failure during El Niño. *Science*, **314**, 115–119, doi:10.1126/science.1131152.

Lee, J. Y., B. Wang, M. C. Wheeler, X. H. Fu, D. E. Waliser, and I. S. Kang, 2013: Real-time multivariate indices for the boreal summer intraseasonal oscillation over the Asian summer monsoon region. *Climate Dyn.*, **40**, 493–509, doi:10.1007/s00382-012-1544-4.

Li, T., B. Wang, C. P. Chang, and Y. Zhang, 2003: A theory for the Indian Ocean dipole–zonal mode. *J. Atmos. Sci.*, **60**, 2119–2135, doi:10.1175/1520-0469(2003)060<2119:ATFTIO>2.0.CO;2.

Lian, T., D. Chen, Y. Tang, and B. Jin, 2014: A theoretical investigation of the tropical Indo-Pacific tripole mode. *Sci. China Earth Sci.*, **57**, 174–188, doi:10.1007/s11430-013-4762-7.

Liebmann, B., and C. A. Smith, 1996: Description of a complete (interpolated) outgoing longwave radiation dataset. *Bull. Amer. Meteor. Soc.*, **77**, 1275–1277.

Matthews, A. J., 2008: Primary and successive events in the Madden–Julian oscillation. *Quart. J. Roy. Meteor. Soc.*, **134**, 439–453, doi:10.1002/qj.224.

Murtugudde, R., and A. J. Busalacchi, 1999: Interannual variability of the dynamics and thermodynamics of the tropical Indian Ocean. *J. Climate*, **12**, 2300–2326, doi:10.1175/1520-0442(1999)012<2300:IVOTDA>2.0.CO;2.

——, J. P. McCreary, and A. J. Busalacchi, 2000: Oceanic processes associated with anomalous events in the Indian Ocean with relevance to 1997–1998. *J. Geophys. Res.*, **105**, 3295–3306, doi:10.1029/1999JC900294.

Pujiana, K., J. N. Moum, W. D. Smyth, and S. J. Warner, 2015: Distinguishing ichthyogenic turbulence from geophysical turbulence. *J. Geophys. Res. Oceans*, **120**, 3792–3804, doi:10.1002/2014JC010659.

Reynolds, R. W., T. M. Smith, C. Liu, D. B. Chelton, K. S. Casey, and M. G. Schlax, 2007: Daily high-resolution-blended analyses for sea surface temperature. *J. Climate*, **20**, 5473–5496, doi:10.1175/2007JCLI1824.1.

Sabeerali, C. T., S. A. Rao, R. S. Ajayamohan, and R. Murtugudde, 2012: On the relationship between Indian summer monsoon withdrawal and Indo-Pacific SST anomalies before and after 1976/1977 climate shift. *Climate Dyn.*, **39**, 841–859, doi:10.1007/s00382-011-1269-9.

——, ——, G. George, D. N. Rao, S. Mahapatra, A. Kulkarni, and R. Murtugudde, 2014: Modulation of monsoon intraseasonal oscillations in the recent warming period. *J. Geophys. Res. Atmos.*, **119**, 5185–5203, doi:10.1002/2013JD021261.

Saji, N. H., and T. Yamagata, 2003: Structure of SST and surface wind variability during Indian Ocean dipole mode events: COADS observations. *J. Climate*, **16**, 2735–2751, doi:10.1175/1520-0442(2003)016<2735:SOSASW>2.0.CO;2.

——, B. N. Goswami, P. N. Vinayachandran, and T. Yamagata, 1999: A dipole mode in the tropical Indian Ocean. *Nature*, **401**, 360–363.

Schneider, T., T. Bischoff, and G. H. Haug, 2014: Migrations and dynamics of the intertropical convergence zone. *Nature*, **513**, 45–53, doi:10.1038/nature13636.

Schott, F. A., and J. P. McCreary, 2001: The monsoon circulation of the Indian Ocean. *Prog. Oceanogr.*, **51**, 1–123, doi:10.1016/S0079-6611(01)00083-0.

Seo, K.-H., and K.-Y. Kim, 2003: Propagation and initiation mechanisms of the Madden-Julian oscillation. *J. Geophys. Res.*, **108**, 4384, doi:10.1029/2002JD002876.

Shukla, R. P., 2014: The dominant intraseasonal mode of intraseasonal South Asian summer monsoon. *J. Geophys. Res. Atmos.*, **119**, 635–651, doi:10.1002/2013JD020335.

Straub, K. H., 2013: MJO initiation in the real-time multivariate MJO index. *J. Climate*, **26**, 1130–1151, doi:10.1175/JCLI-D-12-00074.1.

Suhas, E., J. M. Neena, and B. N. Goswami, 2013: An Indian monsoon intraseasonal oscillations (MISO) index for real time monitoring and forecast verification. *Climate Dyn.*, **40**, 2605–2616, doi:10.1007/s00382-012-1462-5.

Takayabu, Y. N., S. Shige, W.-K. Tao, and N. Hirota, 2010: Shallow and deep latent heating modes over tropical oceans observed with TRMM PR spectral latent heating data. *J. Climate*, **23**, 2030–2046, doi:10.1175/2009JCLI3110.1.

Trenberth, K. E., 1997: The definition of El Niño. *Bull. Amer. Meteor. Soc.*, **78**, 2771–2777, doi:10.1175/1520-0477(1997)078<2771:TDOENO>2.0.CO;2.

——, and D. P. Stepaniak, 2001: Indices of El Niño evolution. *J. Climate*, **14**, 1697–1701, doi:10.1175/1520-0442(2001)014<1697:LIOENO>2.0.CO;2.

Tulich, S. N., and B. E. Mapes, 2008: Multiscale convective wave disturbances in the tropics: Insights from a two-dimensional cloud-resolving model. *J. Atmos. Sci.*, **65**, 140–155, doi:10.1175/2007JAS2353.1.

Uppala, S. M., and Coauthors, 2005: The ERA-40 Re-Analysis. *Quart. J. Roy. Meteor. Soc.*, **131**, 2961–3012, doi:10.1256/qj.04.176.

Valsala, V., 2008: First and second baroclinic mode responses of the tropical Indian Ocean to interannual equatorial wind anomalies. *J. Oceanogr.*, **64**, 479–494, doi:10.1007/s10872-008-0041-1.

Vecchi, G. A., and D. E. Harrison, 2002: Monsoon breaks and subseasonal sea surface temperature variability in the Bay of Bengal. *J. Climate*, **15**, 1485–1493, doi:10.1175/1520-0442(2002)015<1485:MBASSS>2.0.CO;2.

Waliser, D. E., 2006: Intraseasonal variability. *The Asian Monsoon*, B. Wang, Ed., Springer, 203–257.

Wang, B., and H. Rui, 1990: Synoptic climatology of transient tropical intraseasonal convection anomalies: 1975–1985. *Meteor. Atmos. Phys.*, **44**, 43–61, doi:10.1007/BF01026810.

——, and X. Xie, 1997: A model for the boreal summer intraseasonal oscillation. *J. Atmos. Sci.*, **54**, 72–86, doi:10.1175/1520-0469(1997)054<0072:AMFTBS>2.0.CO;2.

——, and Coauthors, 2009: Advance and prospectus of seasonal prediction: Assessment of the APCC/CliPAS 14-model ensemble retrospective seasonal prediction (1980–2004). *Climate Dyn.*, **33**, 93–117, doi:10.1007/s00382-008-0460-0.

——, B. Xiang, J. Li, P. J. Webster, M. N. Rajeevan, J. Liu, and K.-J. Ha, 2015: Rethinking Indian monsoon rainfall prediction in the context of recent global warming. *Nat. Commun.*, **6**, 7154, doi:10.1038/ncomms8154.

Webster, P. J., 1983: Mechanisms of monsoon low-frequency variability: Surface hydrological effects. *J. Atmos. Sci.*, **40**, 2110–2124, doi:10.1175/1520-0469(1983)040<2110:MOMLFV>2.0.CO;2.

——, and C. Hoyos, 2004: Prediction of monsoon rainfall and river discharge on 15–30-day time scales. *Bull. Amer. Meteor. Soc.*, **85**, 1745–1765, doi:10.1175/BAMS-85-11-1745.

——, V. O. Magana, T. N. Palmer, J. Shukla, R. A. Tomas, M. Yanai, and T. Yasunari, 1998: Monsoons: Processes, predictability, and the prospects for prediction. *J. Geophys. Res.*, **103**, 14 451–14 510, doi:10.1029/97JC02719.

Wheeler, M. C., and H. H. Hendon, 2004: An all-season real-time multivariate MJO index: Development of an index for monitoring and prediction. *Mon. Wea. Rev.*, **132**, 1917–1932, doi:10.1175/1520-0493(2004)132<1917:AARMMI>2.0.CO;2.

Wu, G., Y. Liu, B. He, Q. Bao, A. Duan, and F.-F. Jin, 2012: Thermal controls on the Asian summer monsoon. *Sci. Rep.*, **2**, 404, doi:10.1038/srep00404.

Xi, J., L. Zhou, R. Murtugudde, and L. Jiang, 2015: Impacts of intraseasonal SST anomalies on precipitation during Indian summer monsoon. *J. Climate*, **28**, 4561–4575, doi:10.1175/JCLI-D-14-00096.1.

Yang, J., Q. Liu, S.-P. Xie, Z. Liu, and L. Wu, 2007: Impact of the Indian Ocean SST basin mode on the Asian summer monsoon. *Geophys. Res. Lett.*, **34**, L02708, doi:10.1029/2006GL028571.

——, ——, Z. Liu, L. Wu, and F. Huang, 2009: Basin mode of Indian Ocean sea surface temperature and Northern Hemisphere circumglobal teleconnection. *Geophys. Res. Lett.*, **36**, L19705, doi:10.1029/2009GL039559.

Yano, J.-I., and J. L. McBride, 1998: An aquaplanet monsoon. *J. Atmos. Sci.*, **55**, 1373–1399, doi:10.1175/1520-0469(1998)055<1373:AAM>2.0.CO;2.

Yasunari, T., 1980: A quasi-stationary appearance of 30 to 40 day period in the cloudiness fluctuations during the summer monsoon over India. *J. Meteor. Soc. Japan*, **58**, 225–229.

Zhang, C. D., 2005: Madden-Julian oscillation. *Rev. Geophys.*, **43**, RG2003, doi:10.1029/2004RG000158.

——, and J. Ling, 2012: Potential vorticity of the Madden–Julian oscillation. *J. Atmos. Sci.*, **69**, 65–78, doi:10.1175/JAS-D-11-081.1.

Zhang, M., L. Zhou, H. Fu, L. Jiang, and X. Zhang, 2016: Assessment of intraseasonal variabilities in China Ocean Reanalysis (CORA). *Acta Oceanol. Sin.*, **35**, 90–101, doi:10.1007/s13131-016-0820-2.

Zhao, C., T. Li, and T. Zhou, 2013: Precursor signals and processes associated with MJO initiation over the tropical Indian Ocean. *J. Climate*, **26**, 291–307, doi:10.1175/JCLI-D-12-00113.1.

Zhou, L., and R. Murtugudde, 2010: Influences of Madden–Julian oscillations on the eastern Indian Ocean and the Maritime Continent. *Dyn. Atmos. Oceans*, **50**, 257–274, doi:10.1016/j.dynatmoce.2009.12.003.

——, and ——, 2014: Impact of northward-propagating intraseasonal variability on the onset of Indian summer monsoon. *J. Climate*, **27**, 126–139, doi:10.1175/JCLI-D-13-00214.1.